A wireless slot-antenna integrated temperature-pressure-humidity sensor loaded with CSRR for harsh-environment applications

Kou, Hairong; Tan, Qiulin; Wang, Yi; Zhang, Guangjin; Su, Shujing; Xiong, Jijun

DOI:
10.1016/j.snb.2020.127907

Document Version
Peer reviewed version

Citation for published version (Harvard):
Kou, H, Tan, Q, Wang, Y, Zhang, G, Su, S & Xiong, J 2020, 'A wireless slot-antenna integrated temperature-pressure-humidity sensor loaded with CSRR for harsh-environment applications', *Sensors and Actuators B: Chemical*, vol. 311, 127907. https://doi.org/10.1016/j.snb.2020.127907

Journal Pre-proof

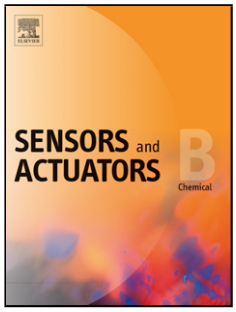

A wireless slot-antenna integrated temperature-pressure-humidity sensor loaded with CSRR for harsh-environment applications

Hairong Kou (Conceptualization) (Methodology) (Software) (Writing - original draft), Qiulin Tan (Supervision), Yi Wang (Writing - review and editing), Guangjin Zhang (Data curation), Shujing Su (Software) (Validation), Jijun Xiong (Supervision)

PII: S0925-4005(20)30254-9

DOI: https://doi.org/10.1016/j.snb.2020.127907

Reference: SNB 127907

To appear in: *Sensors and Actuators: B. Chemical*

Received Date: 18 November 2019

Revised Date: 12 February 2020

Accepted Date: 20 February 2020

Please cite this article as: Kou H, Tan Q, Wang Y, Zhang G, Su S, Xiong J, A wireless slot-antenna integrated temperature-pressure-humidity sensor loaded with CSRR for harsh-environment applications, *Sensors and Actuators: B. Chemical* (2020), doi: https://doi.org/10.1016/j.snb.2020.127907

A wireless slot-antenna integrated temperature-pressure-humidity sensor loaded with CSRR for harsh-environment applications

Hairong Kou[1,2], Qiulin Tan[1,*], Yi Wang[2], Guangjin Zhang[1], Shujing Su[1], Jijun Xiong[1]

[1] Science and Technology on Electronic Test and Measurement Laboratory, North University of China, Tai Yuan 030051, China;

[2] Department of Electronic, Electrical and Systems Engineering, University of Birmingham, Birmingham B15 2TT, U.K.

*Correspondence: tanqiulin@nuc.edu.cn;

Highlights:

- A wireless slot-antenna integrated TPH sensor loaded with CSRR for harsh-environment applications was designed by HFSS.
- The sensor was fabricated on the HTCC substrate and used for harsh environment applications.
- The humidity sensing with GO@PI composite exhibited ultrahigh sensitivity.
- The as-prepared TPH sensor can monitor TPH simultaneously at the high-temperature environment.
- A temperature correction algorithm used for harsh environments was proposed.

Abstract: In this study, a wireless slot-antenna integrated temperature-pressure-humidity (TPH) sensor loaded with complementary split ring resonator (CSRR) for harsh-environment applications was

presented. The sensor is a multi-resonance structure with three separate resonant frequencies, which renders simultaneous measurements of temperature, pressure and humidity by placing sensitive elements in the corresponding CSRR structures. The sensitivity mechanisms for the temperature, pressure and humidity sensing are described in detail. The sensor was customized and fabricated on the high temperature co-fired ceramics (HTCC) using the three-dimensional co-firing and screen-printing technology. The humidity-sensitive graphene oxide modified polyimide (GO@PI) was used and characterized by the scanning electron microscope (SEM) and energy dispersive spectrometry (EDS). The as-prepared TPH sensor can stably work at the ambient environment of 25 - 300 ℃, 10 - 300 kPa, and 20 - 90%RH. The temperature sensitivity of the TPH sensor is 133 kHz/℃. The frequency shift of the pressure sensor is 30 MHz with a highest sensitivity of 107.78 kHz/kPa at 60 %RH, and 300℃. The humidity sensor realizes a sensitivity of 389 kHz/%RH in the low humidity of 20 - 60 %RH and 1.52 MHz/%RH in the high humidity of 60 - 90 %RH at 10 kPa, and 25 ℃. The sensor described in this study has the advantages of simple structure, higher sensitivity, and lower environmental interference and has the potential for utilization in simultaneous TPH monitoring in harsh environments.

Keywords: Slot-antenna, CSRR, wireless TPH sensor, harsh environment.

1. Introduction

Multi-parameters (e.g., temperature, pressure, humidity) measurement in harsh environments, such as industrial pipelines monitoring [1-2], preservation of inflammable and explosive goods [3-4], and mine environmental monitoring [5-6], is extremely important for the efficient operation of equipment and the safety of workers. For example, excessive temperature and pressure on oil or gas sealed pipelines can cause the pipelines to burst, resulting in loss of life and property. Real-time monitoring of temperature, pressure and humidity in the environments can ensure the inflammable and explosive materials are stored

safely. However, the sensing environments for the aforementioned scenarios are often harsh with airtightness, explosions, and high temperature. The traditional wired measurements [7-8] are prone to electric sparks and cannot be used safely in confined space, restricting their application in harsh environments. Wireless and passive measurements have been developed as a reliable and promising method for parameter acquisition in these cases. Various sensing working mechanisms have been applied, such as surface acoustic wave (SAW) [9-10], LC resonance [11-13], and microwave scattering technique (MST) [14-16].

MST is a promising candidate for monitoring TPH in harsh environments, due to its advantages of high sensitivity, accuracy and Q factor [17-18], small volume and low profile, and possibility of monolithic integration. Our group has been researching in the field of high-temperature sensors [19-21] for many years. Among the most notable is an LC wireless passive TPH sensor [19] based on low-temperature co-fired ceramic technology for harsh TPH monitoring, which can operate in an environment of 25 - 200 ℃, 70 - 220 kPa, and 24 - 90 %RH with sensitivities of 3.25 kHz/kPa (pressure), 9.143 kHz/℃ (temperature), and 200 kHz/%RH (at a high humidity range of 60 - 90 %RH). However, this TPH sensor has the shortcomings of low sensitivity and being prone to substantial interference from the metal background. On account of the above considerations and owing to the advantages of MST, the wireless sensors based on MST have increasingly attracted the researchers interests [22-24]. Mohammad [22] designed a planar microwave resonator sensor to detect coating breaches in industrial steel pipelines that can wirelessly transmit signals using an external antenna. In both works [25], [26], an external antenna also used to acquire parameters wirelessly. However, this wireless transmission mode using external antennas requires excessive volume. Antenna integrated sensor [27-31] is a novel technology with potentials for wireless monitoring of parameters in harsh environments. It miniaturizes the sensor system

by embedding the sensitive element inside the substrate of antenna, and perceives the ambient environment through the resonant frequency change of the antenna. A wireless temperature sensor based on split-ring resonator or slot antenna has been reported in previous studies in [16], [32], which can work in high-temperature environments. Later, a wireless pressure sensor was developed in [14] and [15], measuring the pressure based on the resonant frequency change of a sensor loaded with the cylindrical re-entrant resonator. Although these mentioned sensors show excellent performances and high operating temperature, due to low integration level and simple structure, they can only measure a single parameter. CSRR has been considered a promising alternative to realize the multi-sensor capability because of the monolithic integration by embedding it in a metal ground. Moreover, a sensor combined with a CSRR has been confirmed to easily realize miniaturization [33]. Graphene oxide modified polyimide(GO@PI) is sensitive to humidity and stable in high-temperature environments, compared with other materials [34-37]. Thus, GO@PI could be an attractive sensitive material to detect humidity in harsh environments. To date, the CSRR-based wireless TPH sensors for harsh environment monitoring have not been reported.

Herein, we demonstrated a TPH sensor integrated with the slot antenna for wireless detection in harsh environments, which is used for TPH monitor by arranging sensitive elements for its corresponding CSRR structures. The working principle of the TPH sensor was elaborated via circuit analysis and the sensor was optimized by high frequency structure simulator (HFSS) for the realization of three separate resonant frequencies. The morphology and nanostructure of GO@PI were characterized by SEM, and EDS measurements. The as-prepared sensor can stably work at the ambient environment of 25 - 300 ℃, 10 - 300 kPa, and 20 - 90 %RH, which has the potential for utilization in simultaneous TPH monitoring in harsh environments.

2. Working principle and sensor structure

2.1 *Working principle of wireless TPH sensor*

The TPH sensor consists of three parts: pressure sensing, temperature sensing, and humidity sensing, as shown in Fig. 1(a). Each sensing element includes a slot antenna for signal transmission and a CSRR with the corresponding sensing structure for detecting the external environment. The CSRR of the pressure sensing element is placed above the sealed cavity. The GO@PI composite is spin-coated on the CSRR of the humidity sensing element. The structure of the single sensing element is illustrated in Fig. 1(b).

The SIW structure, composed of parallel metal surfaces and metallized holes embedded in the substrate, has the advantages of high Q factor, low environmental interference, and low insertion loss. The radiation losses will occur due to the electromagnetic field leakage inside the SIW, when the hole-spacing is too large. The leakage through the hole-array is minimal as long as the parameters of the SIW meet the following conditions [38]:

$$D < 0.2\lambda_g, p < 2D \quad (1)$$

where, p is the center-to-center separation between the two adjacent metal holes, D is the diameter of the metal holes, and λ_g is the guided wavelength.

Antennas that can be integrated in sensors for wireless signal transmission include patch antenna, and slot antenna. Among them, slot antenna is an ideal candidate due to its advantage of low profile, possibility of multi-frequency integration, and being easily conformed to the surface of the devices. A slot antenna is seamlessly integrated on the sensor in this work to facilitate wireless access. CSRR embedded in the metal ground, not only can miniaturize the sensor at the same frequency to avoid the use of expensive test equipment, but also realize multiple separated frequencies through parameter modulation. The SIW resonator combined with a CSRR structure can obtain a higher Q factor to improve

the sensitivity and resolution of the sensor.

The schematic of the wireless transmission mechanism and TPH sensor is illustrated in Fig. 2(a). The TPH sensor is designed to have three separate resonant frequencies by adjusting the size of the CSRR to monitor temperature, pressure, and humidity, respectively. A waveguide antenna acted as an interrogation antenna illuminates the TPH sensor with signals containing the self-resonance frequencies of the TPH sensor. When the transmitted frequency is the same as the self-resonance frequency of the sensor, the specific electromagnetic wave induces continuous oscillations of standing-wave inside the SIW resonator. The slot antenna will reflect other frequencies back to the antenna, because the matched frequency component will decay over time in the SIW resonator. The resonant frequency of TPH sensor is extracted from the measured S11. In this way, the environmental parameters will be deduced through the shift of resonant frequency in S11.

Fig. 1(b) illustrates the equivalent circuit model to characterize the operating principle of multi-parameter sensor. The equivalent circuits marked with “T”, “P”, and “H” are for temperature, pressure, and humidity measurement, respectively. In general, a microwave resonator can be reduced to an RLC circuit and whose resonant frequency is determined by [18]:

$$f_r = \frac{1}{2\pi\sqrt{L_r C_r}} \tag{2}$$

where, f_r represents the resonant frequency of TPH sensor, and *r* is the abbreviated subscripts of the temperature, pressure, and humidity of the sensor. L_r and C_r represent the equivalent inductance and capacitance of the sensor, respectively.

The equivalent capacitance is composed of two parts: coupling capacitance between the upper and lower metal surface (C_i) and the capacitance of the CSRR structure (C_g), which is expressed as Fig 2(b) :

$$C_r = C_i + C_g \tag{3}$$

For temperature-sensing sensor, when the environmental temperature changes, a dielectric constant ε_r of substrate changes accordingly, which causes a change of the equivalent capacitance C_r, resulting a variation in resonant frequency of TPH sensor.

A sealed cavity embedded in the pressure sensor is used as a pressure-sensing element. When the barometric pressure is loaded on the cavity, the distance *d* changes with the cavity deformation. As a result, the capacitance between the upper and lower metal surface C_i changes, resulting in a change in the resonant frequency of pressure sensor. Its distance *d* under the loading pressure is explained as in Eq. (4) [39] and the corresponding capacitance is expressed as in Eq. (5):

$$d = \frac{3P\square a^4(1-\nu^2)}{16Et^3} \tag{4}$$

$$C_i = \frac{\varepsilon_0 \varepsilon_r A}{d} \tag{5}$$

where, ν and E represent Poisson's ratio and Young's modulus of the substrate, P is the loaded pressure, a is the length of square capacitor patch, and t is the thickness of the sensitive film. ε_0, and ε_r are the relative permittivity of vacuum, and permittivity of substrate, respectively. A is the area of the capacitor plates, and d is the distance between the upper and lower capacitor plates.

GO has been considered as a promising humidity-sensing material owing to the large surface-to-volume ratio induced by its porous structure, whose functional groups can easily bond with water molecules to change its electrical parameters (capacitance, or resistance). The imidized PI has a large surface-to-volume ratio (many tiny pores and wrinkles) and many carbonyl groups (C═O) [19, 36] bonded to H^+ in water molecules, and can work in the high-temperature environments. GO@PI nanocomposites exhibits the excellent performances to sense the humidity by mixing the GO and PI, which is more sensitive to humidity than a single material. The GO@PI is spin-coated on the humidity-sensing area. When the ambient humidity changes, the electrical parameters of the material changes [18,

40-42], causing the capacitance of the CSRR to change, resulting in a resonance frequency shift of the humidity sensor. The above-mentioned description is based on the circuit analysis method to study the equivalent circuit model of the humidity sensor. In the following we can also use the electromagnetic field theory to expound the working mechanism of the humidity sensor. When the external humidity changes, the dielectric constant of the GO@PI will be changed accordingly, resulting in a shift of the resonant frequency of the humidity sensor. The resonant frequency shift of the humidity sensor due to dielectric perturbation is given by [43].

$$\frac{\Delta f_h}{f_h} = \frac{\int V_0(\Delta\varepsilon\overrightarrow{E_1}\cdot\overrightarrow{E_0}+\Delta\mu\overrightarrow{H_1}\cdot\overrightarrow{H_0})dV}{\int V_0(\varepsilon_0|\overrightarrow{E_0}|^2+\mu_0|\overrightarrow{H_0}|^2)dV} \quad (6)$$

Where, V_0 is the volume of the cavity, Δf_h is the change of resonant frequency f_h, Δε and Δμ are the change of dielectric constant and permeability, respectively, E_0 and H_0 are electric and magnetic field without disturbance, E_1 and H_1 are electric and magnetic field after disturbance, respectively.

Here, we implemented a sensor with three separate resonant frequencies by adjusting the size of the three CSRRs. By setting corresponding sensitive elements in their respective sensitive areas, multi-parameter measurement in harsh environments can be achieved. The simulated model is established in HFSS, as shown in Fig. 2(a). The sensor is implemented on a HTCC substrate (ε_r = 9.8 and the thickness of h = 1mm) with an embedded sealed cavity. Fig. 2(c) shows the simulated S11 of the TPH sensor. It can be seen from the result that there are three resonant peaks at 2.35 GHz, 2.49 GHz, and 2.64GHz, which corresponds to the resonant frequencies of temperature sensor, humidity sensor, and pressure sensor, respectively. The simulated magnitude of electric field distributions at resonating modes of 2.35 GHz, 2.49 GHz, and 2.64 GHz are displayed in Fig. 2(d). At 2.35 GHz, the electric field distribution identified across the CSRR structure of temperature sensor. Next for 2.49 GHz, electric field distribution is maximally concentrated around the CSRR structure of humidity sensor. It is also noticed that, the

strong concentration of simulated electric field is in the CSRR structure of pressure sensor at 2.64 GHz. We can see each frequency has its corresponding sensing area. Thus, this separation of sensitive areas with corresponding sensitive elements can be used to implement multi-parameter testing.

2.2 Design and simulation of sensor

In order to realize a high Q factor of the sensor, we chose one resonant unit to simulate in HFSS. Smaller S11 can achieve better impedance matching between the interrogation antenna and sensor, resulting in long-range transmission of the signals and higher temperature testing [44-45]. The length L1 of the slot antenna, the length t of the CSRR, the width bw of the CSRR, and the h between the waveguide antenna and the sensor are studied and optimized for a smaller S11 in HFSS. Fig. 3(a) presents the frequency curves with different L1 of the slot antenna. The resonant frequency of the sensor decreases with the increasing L1, and the shift of the resonant frequency is slight with the length L1. Fig. 3(b) shows the variation of resonant frequency with the width bw of the CSRR. The resonant frequency of the sensor increases with the increasing bw. As shown in Fig. 3(c), when length t of the outer resonant ring becomes longer, the resonant frequency of the sensor shifts towards to the low frequency, which is because the longer length of the resonant ring causes the capacitance C_r increase and resulting in a decrease of the resonant frequency, according to the formula $C_r = 4t \bullet C_{pul}$, where C_{pul} is the per unit length capacitance between the resonant rings. At the same time, a small change in length t of CSRR will cause a large deviation in resonance frequency of the sensor. Therefore, we can achieve a design of the sensor with three separate resonant frequencies by adjusting the length t and width bw of the CSRR. Transmission distance is one of the most important parameters to calibrate sensor performance in wireless system. When the distance h between the interrogation antenna and the sensor is 10 mm, a favorable impedance matching between the interrogation antenna and the sensor is identified. As the distance

increases, the signal coupling gradually becomes weaker. When the distance h is 40 mm, and the interrogation antenna cannot receive the echo signal of the sensor, as shown in Fig. 3(d). The dimensions of the slot antenna and CSRR are summarized in Table 1.

3. Sensor fabrication

3.1 The preparation of GO@PI

GO (layer: 1-6, diameter > 5 μm, XIANFENG nanotechnology, Nanjing, China) and PI-5J polyamic acid (PAA) with 1000–2000 cp viscosity (YIDUN Material, Suzhou, China) are the raw materials of the GO@PI. The GO suspension was prepared by dispersing 20 mg GO into the 20 ml ethanol, and using the ultrasonic dispersion at 30 °C for 3 h to weaken the interaction between the GO nanoparticles. Then, 30 ml PAA was added into the GO suspension followed by the magnetic stirring of 1000 r/min at 30 ℃ for 2 h to achieve a uniform dispersion of the GO@PI. The morphology structures and elements distribution of GO@PI nanocomposites were characterized using SEM and EDS, as shown in Fig. 4. The results indicated that the GO nanoflakes are evenly dispersed in PI without aggregations. Meanwhile, the air-holes and wrinkles formed by the evaporation of alcohol were dispersed in the GO@PI composites, which increased the contact area with the water molecules.

3.2 The fabrication of the TPH sensor

Fig. 5(a) illustrates the fabrication process of the TPH sensor. The TPH sensor was constructed using the 99% HTCC green tapes (ESL 44007-A, USA) with a single-layer thickness of 130 μm and the carbon films (ESL 49000, USA) with a thickness of 125 μm based on the high-temperature co-firing technology and screen printing technology. The 8-layers HTCC green tapes were punched to form a specific pattern using a laser drilling machine, where the layers 3 and 4 were patterned with a vacant square of 8 mm × 8 mm. Then, the 2-layer carbon films were filled in the square holes of the layers 3 and 4. Subsequently,

the 8 layers HTCC green tapes with an embedded cavity filled with carbon films were stacked and followed by the lamination process, which is sealed by vacuum packaging under a pressure of 20 MPa at 75 ℃ for 10 min.

After lamination, the monolithic structure was evenly cut into several sensors. The sensor is sintered in a high-temperature environment to increase the strength of the substrate and produce a strong chemical bonding between the green type layers, as the lamination process is a physical bonding and a small external force can separate the green type layers. Afterward, the fabricated sensor is placed in a muffle furnace according to a sintering curve we researched [12-14]. When the temperature rises to between 600 and 700 ℃, the oxygen in the air reacts with the carbon films to form carbon dioxide (CO_2), which is released from the numerous pores of the unsintered green tapes. At the same time, the open environment air enters the cavity to maintain the air-pressure balance of the cavity. To prevent the collapse of the sensitive membrane, this stage is set for 300 minutes to completely burn the carbon films for a hermetic cavity. As the temperature continues to rise until 1500 ℃, the chemical binder in the HTCC green tapes is completely discharged and the ceramic particles are rearranged until they fuse with each other, eventually forming a dense HTCC substrate with a sealed cavity.

The metallized patterns were formed with silver paste by screen printing technology. The air holes were filled with silver paste to realize the metallized array holes. Next, the ready-made sensor is placed in a muffle furnace at 100 ℃ for 15 min to dry the silver paste followed by sintering at a peak temperature of 850 ℃ for 1 h, as demonstrated in our previous work [9,12-14].

The metallized sensor is cooled to room temperature, after which, the as-prepared GO@PI was uniformly dropped on the CSRR for the humidity sensing and then spin coated with a speed of 1500 r/min for 30 s to obtain a thin GO@PI film. Finally, the GO@PI imidization was implemented in a high-

temperature sealed pressure furnace under the nitrogen pressure of 1 bar followed by solidifying with a slow rate of temperature rise (1 ℃/min) and maintaining at 350 ℃ for 2h. This imidization process facilitates the PI to carry more carbonyl groups (C═O). After cooling, the wireless and passive TPH sensor was completed, as shown in Fig. 5(b).

4. Experiment results and analysis

4.1 The platform of measurement

To characterize the performance of the as-prepared sensor, a measurement platform composed of a sealed furnace, JT1500 TPH controller and a network analyzer (E5061B) is custom-made for the precise control of temperature, pressure, and humidity at high-temperature environment, as shown in Fig. 6(a). The reference sensors are installed inside the furnace to feed back its internal environmental parameters in real time. The TPH sensor is placed in the sealed furnace and the waveguide antenna connected to a network analyzer via a coaxial line is faced to the sensor with a distance of 10 mm in order to obtain strong resonance peaks from the sensor. Using this measurement platform, the temperature, pressure, and humidity can be applied to the TPH sensor with precise, simultaneous, and independent control. The actual test platform is shown in Fig. 6(b). Fig. 6(c) shows the measured S11 at an environment of 25 ℃, 10 kPa and 60 %RH. It can be seen from the result that three obvious resonance peaks appear in the S11 curve, corresponding to the resonant frequency of the temperature sensor, humidity sensor, and pressure sensor, respectively, which is well consistent with the simulated result except for the humidity sensing. That is due to the simulation of the TPH sensor without the GO@PI thin film. The GO@PI coated on CSRR of the humidity senor changes the capacitance of the CSRR, resulting a shift in resonant frequency of the humidity sensing.

4.2 Temperature sensing performance

The measured S11 of the wireless TPH sensor at an environment of 10 kPa and 60 %RH were investigated as the temperature increases from 25 ℃ to 300 ℃. Fig. 6(d) displays that the resonant frequencies of the temperature sensor, humidity sensor, and pressure sensor decrease with the increasing temperature. This is due to the increase in the dielectric constant of the HTCC substrate with temperature. The result shown in Fig. 6(e) indicates that the change in resonant frequency of corresponding sensor at the temperature range from 25 ℃ to 300 ℃ is almost linear with the varying temperature, and the temperature sensitivity of the TPH sensor is 133 kHz/℃.

4.3 Pressure Sensing performance

The pressure sensing performance of the TPH sensor was measured at the same humidity level (60 % RH) and different temperatures increasing from 25 ℃ to 300 ℃ with various loading pressure up to 300 kPa. We have measured the sensor in high temperature and high atmospheric pressure environment for three cycles, and the measured data remain almost unchanged. Fig. 7(a) shows the measured S11 for different pressures. It is illustrated that as the pressure increases, the resonant frequency of the pressure sensor reduces significantly whereas the resonant frequencies of the temperature sensor and humidity sensor are barely affected The pressure response curves of the sensor within the barometric pressure of 10 - 300 kPa at 25 °C and 300 °C are shown in Figs. 7(b) and 7(c). The resonant frequency of pressure sensor decreases from 2.66 GHz to 2.64 GHz under a pressure range of 10 - 300 kPa at 25 °C, which is up to 20 MHz. As the temperature raises up to 300 °C, the frequency offset of the pressure sensor is up to 30 MHz in the same pressure range. Furthermore, the resonant frequency points under a pressure range of 10 - 300 kPa and at a temperature range of 25 - 300 ℃ are subsequently extracted and the corresponding linear fitted curves at different temperature are plotted in Fig. 7(d). The pressure sensitivity of the sensor is 63.69 kHz/kPa at 25 ℃, while the sensitivity increases to 107.78 kHz/kPa at 300 ℃. This is due to the

high temperature reduces the hardness of the HTCC substrate, resulting in a large deformation of the cavity and a larger pressure sensitivity.

The pressure sensitivity is obtained only at a few given temperature such as 25 ℃, 50 ℃, 100 ℃, 150 ℃, 200 ℃, 250 ℃ and 300 ℃. For practical application of the TPH sensor, it is necessary to measure an accurate pressure parameter at an arbitrary temperature. Hence, we have analyzed the measured data and found that the results were consistent with the plate model, as shown in Fig. 7(e). The temperature of the harsh environment can be determined according to the temperature sensor discussed in section 4.2. Therefore the pressure at different temperature can be expressed as follows:

$$Z=Z_0+a*x+b*y \tag{5}$$

where, Z_0 = 30675.5405, a = -1.73109, b = -11485.71431. x, y, and Z represents temperature, frequency, and pressure, respectively.

Fig. 7(f) shows the error analysis of the measured average pressure values of the sensor. It can be seen from the result that the measured error values are relatively small at high-temperature and high-pressure environment (150 - 300℃ and 150-300 kPa). Hence, the plane fitted model can be used to extract pressure signals precisely in high-temperature environments.

4.4 Humidity sensing performance

At 25 ℃ and 10 kPa, the humidity performance of the TPH sensor was investigated in a humidity environment ranging from 20 %RH to 90 %RH in a step of 10 %RH for three cycles, as plotted in Fig. 8(a). It is observed that the resonant frequency of the humidity sensor decreases with the increasing humidity, while the resonant frequency of the temperature and pressure senor exhibits no frequency shift. That is to say, the TPH sensor can be used to monitor humidity under a harsh environment. The resonant frequency shift of the humidity sensor is 58 MHz within the range of 20 - 90 %RH, as shown in Fig. 8(b).

We note from Fig. 8(c) that the measured results of humidity sensor can be fitted with the two linear curves in low humidity of 20 - 60 %RH and high humidity of 60 - 90 %RH respectively. The sensitivity of the humidity sensor is 389 kHz/%RH in the low humidity range and 1.52 MHz/%RH in the high humidity. In Fig. 8(e), the humidity sensor had a maximum of 12.6% nonlinearity errors in the range of 20-60 %RH; a maximum of 3.6% nonlinearity errors in the range of 60-90 %RH.

The humidity sensitive mechanism of the GO@PI-based wireless passive humidity sensor is shown schematically in Fig. 8(d). When the sensor is illuminated by the waveguide antenna, the strong electric field is distributed inside the CSRR, as shown in Fig. 2(d). The water molecules adsorbed by the GO@PI are polarized and ionized into protons (H^+) and hydroxide ions (OH^-) by the electric field. Those protons (H^+) were combined with the carbonyl groups (C═O) of GO@PI. Meanwhile, it is well known that GO is a hydrophilic material with many hydrophilic functional groups on its surface, which absorbed water molecules via its dense porous structures owing to a large surface-to-volume ratio. Therefore, the migration of protons (H^+) under the induction of electric field leads to a change in dielectric constant of GO@PI material, which causes a change in capacitance of CSRR structure (C_g), resulting a deviation in resonance frequency of humidity sensor. At lower humidity, ionized protons (H^+) and hydroxide ions (OH^-) are only distributed on the surface of the GO@PI material, which is a discontinuous film. Hence, migration of protons (H^+) is not obvious, resulting in a low sensitivity of the sensor at 20 - 60% RH. As the RH increases, the massive water molecules entered the internal structure of the GO@PI film through the dense micropores and wrinkles formed by the evaporation of ethanol. This process is a bulk phenomenon, which increases the bulk to contact with the GO@PI, facilitating the migration of protons in water molecules. Especially in a higher RH, physisorbed water molecules were ionized by the electric field to form a large number of H_3O^+ scattered throughout the GO@PI to enhance protons adsorption. At

the same time, the Grotthuss mechanism ($H_2O + H_3O^+ \rightarrow H_3O^+ + H_2O$) [14, 35] can enhance the protons transport between adjacent water molecules to expand the electrolytic conduction. In other word, as the dielectric constant of GO@PI film increases sharply with the massive protons migration, the capacitance of CSRR structure increases greatly, which results in a sharp decrease in the resonant frequency of the humidity sensor. Therefore, the sensitivity of 60 - 90 %RH is 1.47 MHz/%RH and higher than that of 20 - 60 %RH.

For practical application, the performances of response time and stability were measured. The 90 %RH environment is set using a humidity chamber (SDJS701B, Chongqing SD Equipment, Chongqing, China). The proposed sensor was first put in the room environment (60 %RH), and then instantly transferred to the 90 %RH environment till the resonant frequency of sensor becomes stable. Repeat this process several times to obtain the response curve of the sensor, as shown in the Fig. 8(f). Cleary, seen from the inset of Fig. 8(f), the response time is 11 s and the recovery time is about 28s. The higher recovery time can be explained by the mechanism of protons transport. The proton-carbonyl separation process is harder than the proton-carbonyl bonding process. The stability of the sensor was tested at 20 %RH, 40 %RH, 70 %RH, and 90 %RH, and the corresponding resonant frequencies were recorded every day for 15 days and plotted in Fig. 8(g). The result indicated that the sensor exhibited good stability.

5. Conclusion

In summary, we demonstrate, for the first time, a wireless slot-antenna integrated TPH sensor loaded with the CSRR and utilize it for wireless simultaneous measurements of temperature, pressure, and humidity in harsh environments. The coupling principle between the TPH sensor and waveguide antenna and the equivalent circuit model of the TPH sensor have been analyzed. The TPH sensor was designed to obtain three separate resonant frequencies. According to the optimized parameters, the sensor was

customized, and fabricated on HTCC substrate using the three-dimensional co-firing technology and screen printing technology. The as-prepared sensor can stably work at the ambient environment of 25 - 300 ℃, 10 - 300 kPa, and 20 - 90%RH. The temperature sensitivity of the TPH sensor is 133 kHz/℃; the frequency shift of the pressure sensor is 30 MHz with a highest sensitivity of 107.78 kHz/kPa at 65 %RH, 300℃; the humidity sensor realizes a sensitivity of 389 kHz/%RH in the low frequency (20 - 60 %RH) and 1.52 MHz/%RH in the high humidity (60 - 90 %RH) at 10 kPa, 25℃. The proposed TPH sensor is significant for mine environmental monitoring. The successful development of such wireless TPH sensor is a major step ahead in harsh environments for wireless multi-parameter measurements.

Credit Author Statement

Hairong Kou: Conceptualization, Methodology, Software, Writing- Original draft preparation

Qiulin Tan: Supervision and Fund provider

Yi Wang: Writing- Reviewing and Editing

Guangjin Zhang: Measurement and Data curation

Shujing Su: Software, Validation

Jijun Xiong: Supervision and Fund provider

Declaration of interests

The authors declare that they have no known competing financial interests or personal relationships that could have appeared to influence the work reported in this paper.

Acknowledgments:

This work was supported by National Natural Science Foundation of China (Grant No. 51875534, U1837209, 61471324, and 51425505,), the Outstanding Young Talents Support Plan of Shanxi province, the Innovative Research Group Project of National Natural Science Foundation of China (Grant No. 51821003), and the Shanxi "1331 project" keys subjects Construction, and in part by National Key R&D Program of China (Grant No. 2018YFB2002503).

Conflicts of Interest:

The authors declare no conflict of interest.

Reference

[1] Ali S, Qaisar S, Saeed H, et al. Network challenges for cyber physical systems with tiny wireless devices: A case study on reliable pipeline condition monitoring. Sensors, 2015, 15(4): 7172-7205.

[2] reza Akhondi M, Talevski A, Carlsen S, et al. The role of wireless sensor networks (WSNs) in industrial oil and gas condition monitoring//4th IEEE International Conference on Digital Ecosystems and Technologies. IEEE, 2010: 618-623.

[3] Townend D T A, Chamberlain E A C. The influence of pressure on the spontaneous ignition and limits of inflammability of ether-air mixtures. Proceedings of the Royal Society of London. Series A-Mathematical and Physical Sciences, 1937, 158(894): 415-429.

[4] Lyu S, Zhang Y, Wang W, et al. Simulation Study on Influence of Natural Gas Pipeline Pressure on Jet Fire//IOP Conference Series: Earth and Environmental Science. IOP Publishing, 2019, 242(2): 022041.

[5] Sengupta M. Environmental impacts of mining monitoring, restoration, and control. Routledge, 2018.

[6] Bui X N, Nguyen H, Le H A, et al. Prediction of blast-induced air over-pressure in open-pit mine: assessment of different artificial intelligence techniques. Natural Resources Research, 2019: 1-21.

[7] Chen Z, Wang Z, Li X, et al. Flexible piezoelectric-induced pressure sensors for static measurements based on nanowires/graphene heterostructures. ACS nano, 2017, 11(5): 4507-4513.

[8] Mannsfeld S C B, Tee B C K, Stoltenberg R M, et al. Highly sensitive flexible pressure sensors with microstructured rubber dielectric layers. Nature materials, 2010, 9(10): 859.

[9] Torsi L, Dodabalapur A, Sabbatini L, et al. Multi-parameter gas sensors based on organic thin-film-transistors. Sensors and Actuators B: Chemical, 2000, 67(3): 312-316.

[10] Della Lucia F, Zambrozi Jr P, Frazatto F, et al. Design, fabrication and characterization of SAW pressure sensors for offshore oil and gas exploration. Sensors and Actuators A: Physical, 2015, 222: 322-328.

[11] Fonseca M A, English J M, Von Arx M, et al. Wireless micromachined ceramic pressure sensor for high-temperature applications. Journal of Microelectromechanical Systems, 2002, 11(4): 337-343.

[12] Tan Q, Lu F, Ji Y, et al. LC temperature-pressure sensor based on HTCC with temperature compensation algorithm for extreme 1100° C applications. Sensors and Actuators A: Physical, 2018, 280: 437-446.

[13] Tan Q, Luo T, Wei T, et al. A wireless passive pressure and temperature sensor via a dual LC resonant circuit in harsh environments. Journal of Microelectromechanical Systems, 2017, 26(2): 351-356.

[14] Su S, Lu F, Wu G, et al. Slot antenna integrated re-entrant resonator based wireless pressure sensor for high-temperature applications. Sensors, 2017, 17(9): 1963.

[15] Cheng H, Shao G, Ebadi S, et al. Evanescent-mode-resonator-based and antenna-integrated wireless passive pressure sensors for harsh-environment applications. Sensors and Actuators A: Physical, 2014, 220: 22-33.

[16] Cheng H, Ebadi S, Ren X, et al. Wireless passive high-temperature sensor based on multifunctional reflective patch antenna up to 1050 degrees centigrade. Sensors and Actuators A: Physical, 2015, 222: 204-211.

[17] Yun T, Lim S. High-Q and miniaturized complementary split ring resonator-loaded substrate integrated waveguide microwave sensor for crack detection in metallic materials. Sensors and Actuators A: Physical, 2014, 214: 25-30.

[18] Chen C M, Xu J, Yao Y. Fabrication of miniaturized CSRR-loaded HMSIW humidity sensors with high sensitivity and ultra-low humidity hysteresis. Sensors and Actuators B: Chemical, 2018, 256: 1100-1106.

[19] Tan Q, Lv W, Ji Y, et al. A LC wireless passive temperature-pressure-humidity (TPH) sensor integrated on LTCC ceramic for harsh monitoring. Sensors and Actuators B: Chemical, 2018, 270: 433-442.

[20] Kou H, Zhang L, Tan Q, et al. Wireless wide-range pressure sensor based on graphene/PDMS sponge for tactile monitoring. Scientific reports, 2019, 9(1): 3916.

[21] Li C, Tan Q, Jia P, et al. Review of research status and development trends of wireless passive LC resonant sensors for harsh environments. Sensors, 2015, 15(6): 13097-13109.

[22] Zarifi M H, Deif S, Abdolrazzaghi M, et al. A microwave ring resonator sensor for early detection of breaches in pipeline coatings. IEEE Transactions on Industrial Electronics, 2017, 65(2): 1626-1635.

[23] Saadat-Safa M, Nayyeri V, Khanjarian M, et al. A CSRR-Based Sensor for Full Characterization of Magneto-Dielectric Materials. IEEE Transactions on Microwave Theory and Techniques, 2019, 67(2): 806-814.

[24] Guo H, Zhu Q, Tang J, et al. A temperature and humidity synchronization detection method based on microwave coupled-resonator. Sensors and Actuators B: Chemical, 2018, 261: 434-440.

[25] Scott S, Peroulis D. A capacitively-loaded MEMS slot element for wireless temperature sensing of up to 300 ℃//Microwave Symposium Digest, 2009. MTT'09. IEEE MTT-S International. IEEE, 2009: 1161-1164.

[26] Jatlaoui M M, Chebila F, Pons P, et al. Working principle description of the wireless passive EM transduction pressure sensor. The European Physical Journal Applied Physics, 2011, 56(01): 13702.

[27] Tiwari N K, Tiwari Y, Akhtar M J. Design of CSRR-Based Electronically Tunable Compact RF Sensor for Material Testing. IEEE Sensors Journal, 2018, 18(18): 7450-7457.

[28] Ndoye M, Kerroum I, Deslandes D, et al. Air-filled substrate integrated cavity resonator for humidity sensing. Sensors and Actuators B: Chemical, 2017, 252: 951-955.

[29] Ndoye M, El Matbouly H, Sama Y N, et al. Sensitivity evaluation of dielectric perturbed substrate integrated resonators for hydrogen detection. Sensors and Actuators A: Physical, 2016, 251: 198-206.

[30] Nosrati M, Abbasi Z, Baghelani M, et al. Locally Strong-Coupled Microwave Resonator Using PEMC Boundary for Distant Sensing Applications. IEEE Transactions on Microwave Theory and Techniques, 2019, 67(10): 4130-4139.

[31] Abbasi Z, Baghelani M, Nosrati M, et al. Real-Time Non-Contact Integrated Chipless RF Sensor for Disposable Microfluidic Applications. IEEE Journal of Electromagnetics, RF and Microwaves in Medicine and Biology, 2019.

[32] Lu F, Tan Q, Ji Y, et al. A novel metamaterial inspired high-temperature microwave sensor in harsh environments. Sensors, 2018, 18(9): 2879.

[33] D.E. Senior, X. Cheng, Y.K. Yoon, Electrically tunable evanescent mode half-mode substrate-integrated-waveguide resonators, IEEE Microw. Wireless Compon. Lett. 22 (2012) 123–125.

[34] Sahatiya P, Kadu A, Gupta H, et al. Flexible, disposable cellulose-paper-based MoS2/Cu2S hybrid for wireless environmental monitoring and multifunctional sensing of chemical stimuli. ACS applied materials & interfaces, 2018, 10(10): 9048-9059.

[35] Guo H, Lan C, Zhou Z, et al. Transparent, flexible, and stretchable WS_2 based humidity sensors for electronic skin. Nanoscale, 2017, 9(19): 6246-6253.

[36] Ranjan P, Tiwary P, Chakraborty A K, et al. Graphene oxide based free-standing films for humidity and hydrogen peroxide sensing. Journal of Materials Science: Materials in Electronics, 2018, 29(18): 15946-15956.

[37] Zhang D, Wang M, Yang Z. Facile fabrication of graphene oxide/Nafion/indium oxide for humidity sensing with highly sensitive capacitance response. Sensors and Actuators B: Chemical, 2019, 292: 187-195.

[38] Cassivi Y, Perregrini L, Arcioni P, et al. Dispersion characteristics of substrate integrated rectangular waveguide. IEEE Microwave and Wireless components letters, 2002, 12(9): 333-335.

[39] Timoshenko S, Woinowsky-Krieger S. Theory of plates and shells. 2nd ed. McGraw-Hill, 1959.

[40] Kim Y H, Jang K, Yoon Y J, et al. A novel relative humidity sensor based on microwave resonators and a customized polymeric film. Sensors and Actuators B: Chemical, 2006, 117(2): 315-322.

[41] Manzari S, Occhiuzzi C, Nawale S, et al. Humidity sensing by polymer-loaded UHF RFID antennas. IEEE Sensors Journal, 2012, 12(9): 2851-2858.

[42] Amin E M, Bhuiyan M S, Karmakar N C, et al. Development of a low cost printable chipless RFID humidity sensor. IEEE sensors Journal, 2013, 14(1): 140-149.

[43] M. S. Boybay and O. M. Ramahi, Material characterization using complementary split-ring resonators. IEEE Trans. Instrum. Meas., vol. 61, no. 11, pp. 3039–3046, Nov. 2012.

[44] Liu W, Xu L, Zhan H. Design of 2.4 GHz/5 GHz planar dual-band electrically small slot antenna based on impedance matching circuit. AEU-International Journal of Electronics and Communications, 2018, 83: 322-328.

[45] P. W. Hannan, D. S. Lerner, and G. H. Knittel. Impedance matching a phased array-antenna over wide scan angles by connected circuits. IEEE Trans. Antennas Propag., vol. 13, no. 1, pp. 28–34, Jan. 1964.

Biographies

Hairong Kou is currently in the graduate program at North University of China to pursue her Ph.D degree, Shanxi, China, since 2016. Her research interests concentrate on design and production of wireless and passive sensor used in harsh environment. She is a visiting student at the University of Birmingham.

Qiulin Tan received his B.S., M.S. and Ph.D degrees from North University of China, Shanxi, China, in 2002, 2006, and 2009 respectively, and now he has finished studying in Tsinghua University as a post-doctor in 2015. He is a senior member of IEEE. He is a professor and doctoral supervisor in North university of China. He won 3 State/Ministerial Prize for Progress in Science and Technology in China. He has launched over 80 papers and one book. His current research interests include nanomaterials, IR gas sensor, wireless passive micro-sensors, smart flexible sensor and measuring instrument.

Yi Wang (M'09–SM'12) was born in Shandong, China. He received the B.Sc. degree in physics and M.Sc. degree in condensed matter physics from the University of Science and Technology, Beijing, China, in 1998 and 2001, respectively, and the Ph.D. degree in electronic and electrical engineering from the University of Birmingham, Edgbaston, Birmingham, U.K., in 2005. In 2011, he became a Senior Lecturer and then Reader at the University of Greenwich. In 2018, Yi joined Birmingham as a Senior Lecturer.

His current research interests include millimeter-wave and terahertz devices for metrology, communications and sensors, micromachining, microwave circuits based on multiport filtering networks, and filter-antenna integration.

Guangjin Zhang received his B.S. degrees from Zhongyuan University of Technology, Zhengzhou, China, in 2017. He is currently in the graduate program at North University of China to pursue his M.S. degree. His research interest is LC resonant sensor under harsh environments and radio frequency circuit.

Shujing Su received her BSc and MSc degrees in electrical engineering from North University of China in Shanxi, China, in 1994 and 2000, and PhD degree in electromechanical engineering from Beijing Institute of Technology in Beijing, China in 2008. She is a professor and doctoral supervisor in North university of China. The main research direction is wireless passive micro-nano sensors in harsh environment.

JijunXiong received his B.S. and M.S. degrees in electrical engineering from North University of China in Shanxi, China, in 1993 and 1998, and PhD degree in Precision Instruments and Mechanology from Tsinghua University in Beijing, China, in 2003.His research interest is in the fields of measurement and MEMS.

Table I. Detailed parameters of the designed sensor

Parameter	Meaning	Value (mm)	Parameter	Meaning	value (mm)
W	The width of substrate	28	t_t	The length of temperature CSRR	9
L	The length of substrate	84	t_p	The length of pressure CSRR	8
W1	The width of slot antenna	2	t_h	The length of humidity CSRR	8.5
L1	The length of slot antenna	21	p	The gap between adjacent metal holes	2
lw	The gap between resonant ring	1.5	g	The gap of CSRR	1
bw	The width of CSRR	1.4	D	The diameter of metal holes	1

Figure captions

Fig. 1. (a) Schematic of the TPH sensor. (b) The structure of a single sensing element in the TPH sensor.

Fig. 2. (a) Wireless sensing mechanism of the TPH sensor. (b) Schematic and circuit model of the wireless TPH sensor. (c) The simulated S11 of as-designed TPH sensor based on HFSS. (d) The simulated electric field at 2.35 GHz, 2.49 GHz, and 2.64 GHz.

Fig. 3. HFSS simulation of (a) the length L1 of slot antenna; (b) the width bw of the CSRR; (c) the length t of the CSRR; (d) the distance h between the sensor and the waveguide antenna.

Fig. 4. (a)The SEM image of GO@PI. (b) The side view SEM image of GO@PI. (c) The EDS of GO@PI.

Fig. 5. (a) The process of TPH sensor fabrication. (b) Photograph of the as-prepared TPH sensor.

Fig. 6. (a) The schematic diagram of measurement platform. (b) The measurement platform for measure the TPH parameters. (c) The measured S11 of as-prepared TPH sensor. (d) Temperature response curves of the TPH sensor at temperature range of 25 – 300 ℃. (e) Temperature versus frequency curves of the temperature, pressure, and humidity sensor.

Fig. 7. (a) Measured S11 curve of the TPH sensor at 25 ℃, 65 %RH, and 10 - 300 kPa. The S11 curve of pressure sensor at (b) 25 ℃, 65 %RH, and 10 - 300 kPa; (c) 300 ℃, 65 %RH, and 10 - 300 kPa. (d) Pressure versus frequency curve of the pressure sensor at different temperatures within 10-300 kPa. (e) The plane model for pressure at different temperature. (f) The measured error with the plane fitted model.

Fig. 8. (a) Measured S11 curve of TPH sensor at 25 ℃, 10 kPa, and 20 - 90 %RH. (b) The S11 curve of humidity sensor at 25 ℃, 10 kPa, and 20 - 90 %RH. (c) Humidity versus frequency curve of the humidity sensor within 20 - 90 %RH. (d) Sensing mechanism of humidity sensor. (e) The measured error with the fitted curve. (f) The response and recovery time of GO@PI film based humidity sensor. (g) The stability of GO@PI film based humidity sensor.

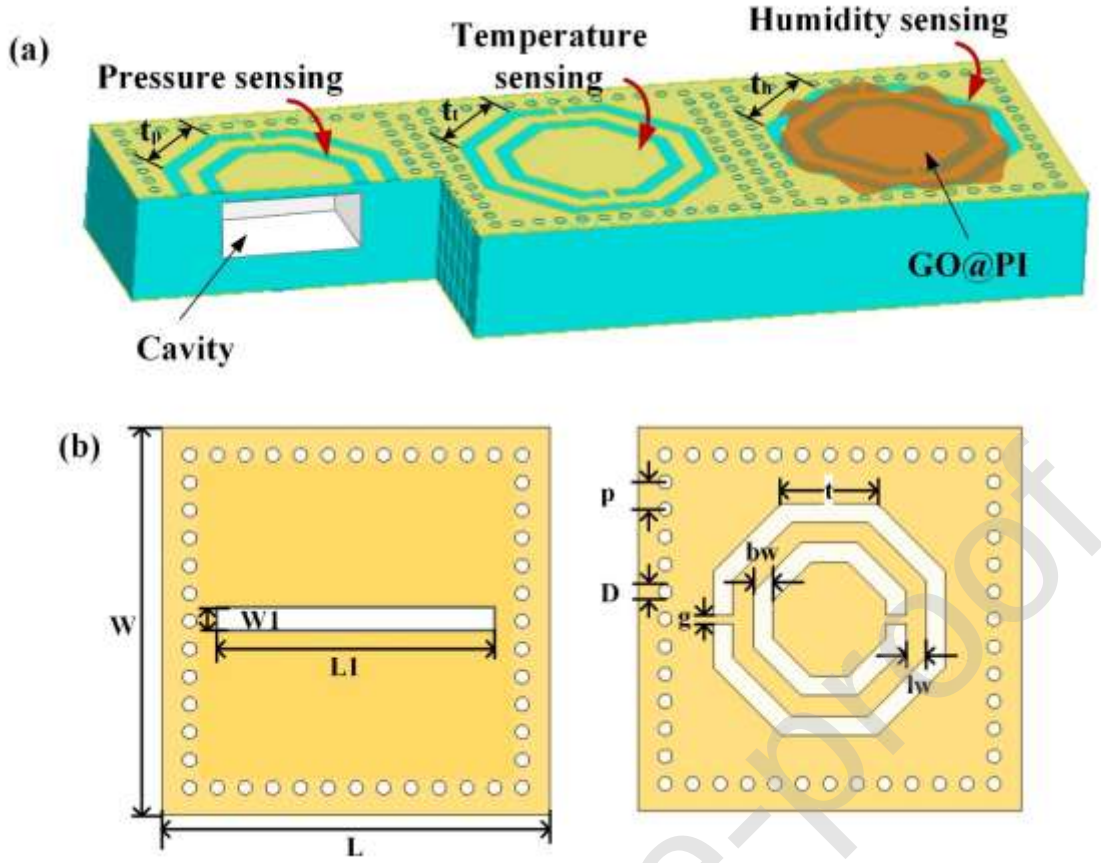

Figure 1.

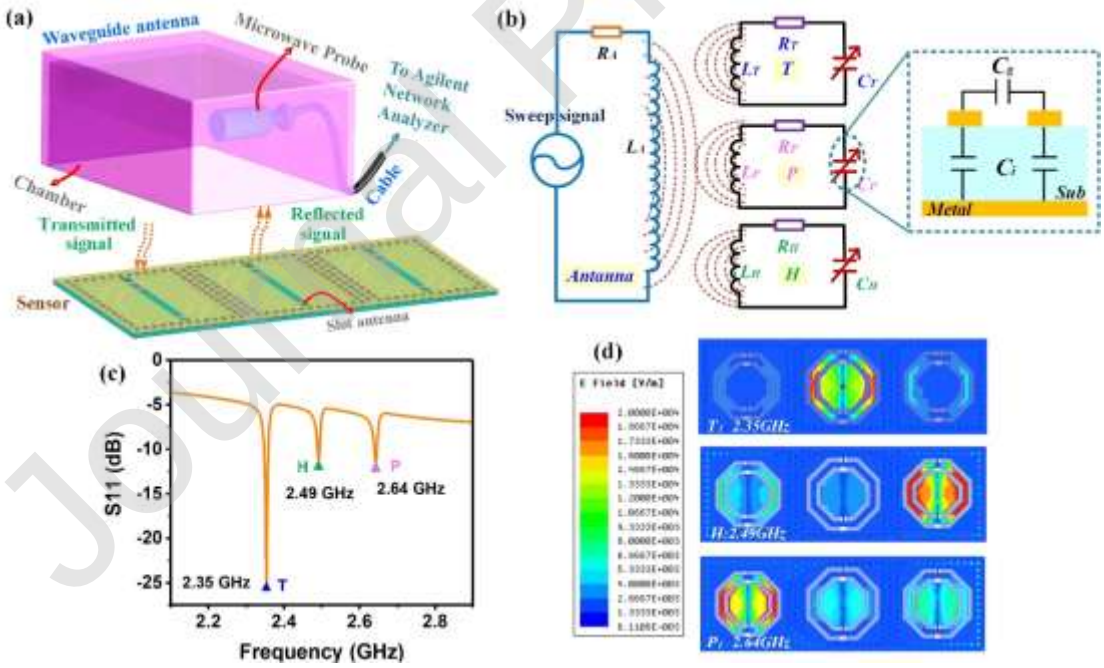

Figure 2.

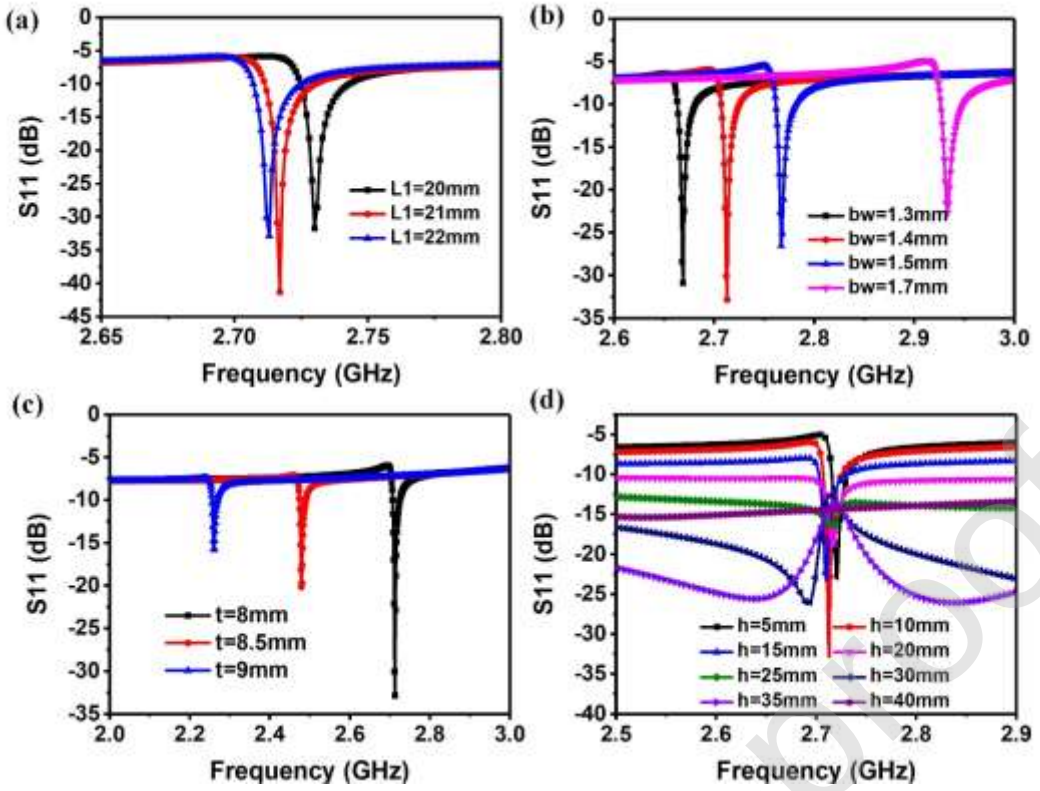

Figure 3.

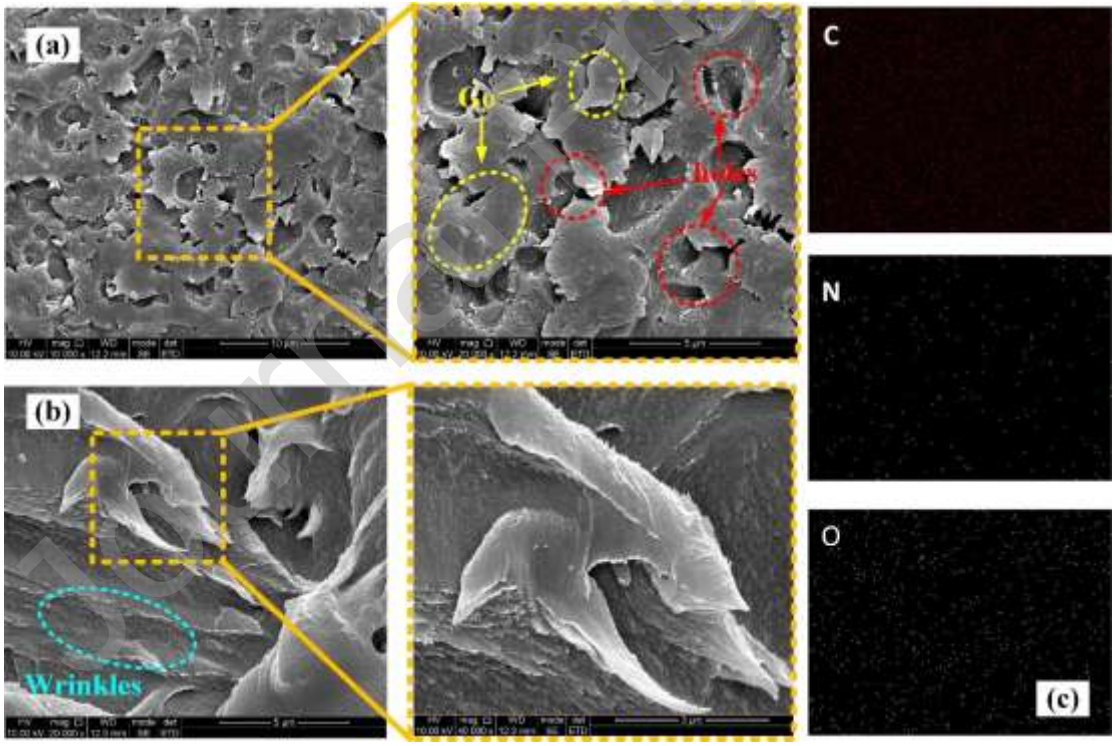

Figure 4.

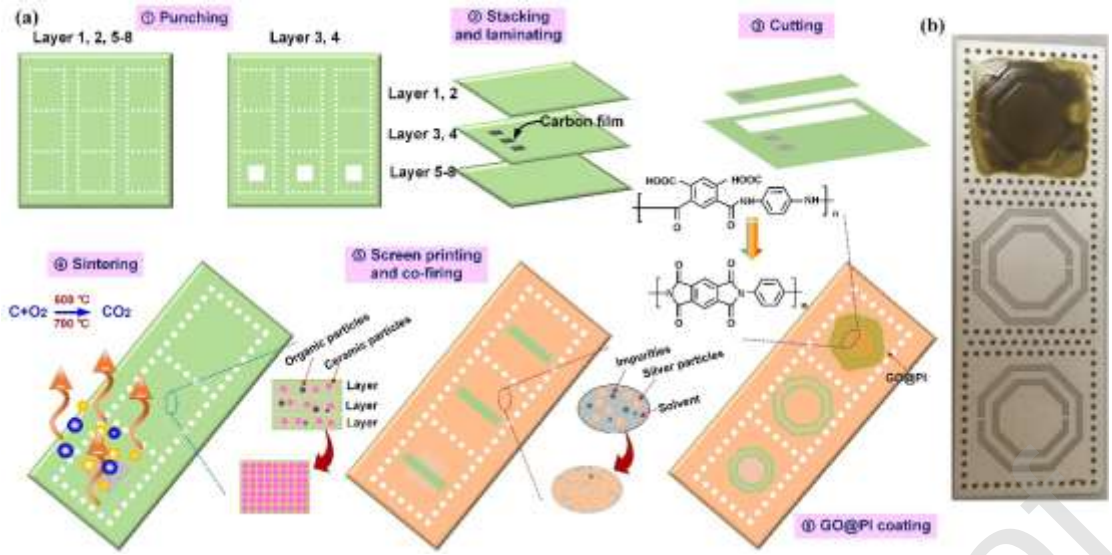

Figure 5.

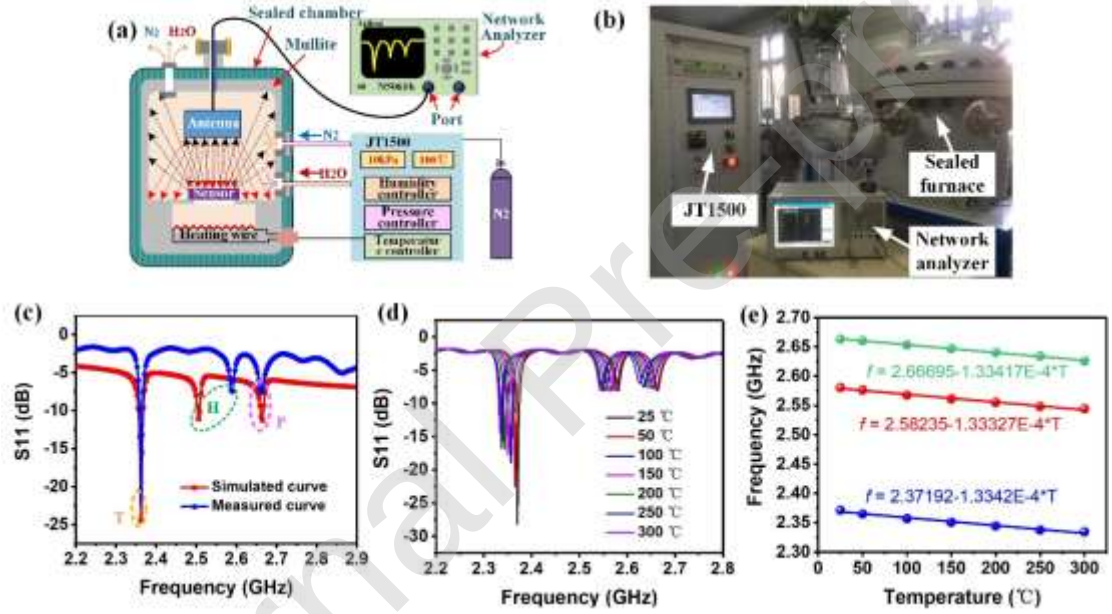

Figure 6.

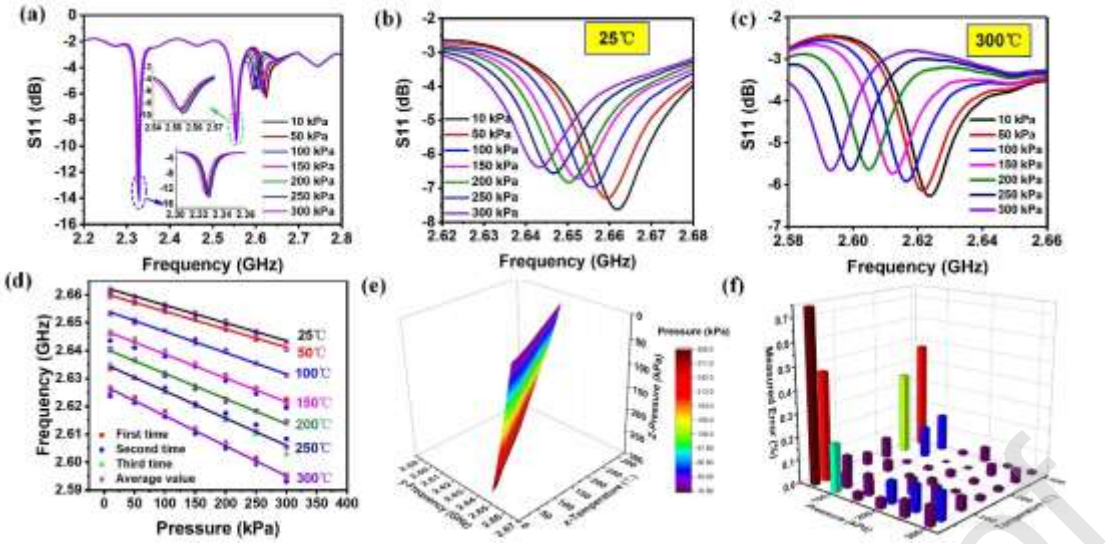

Figure 7.

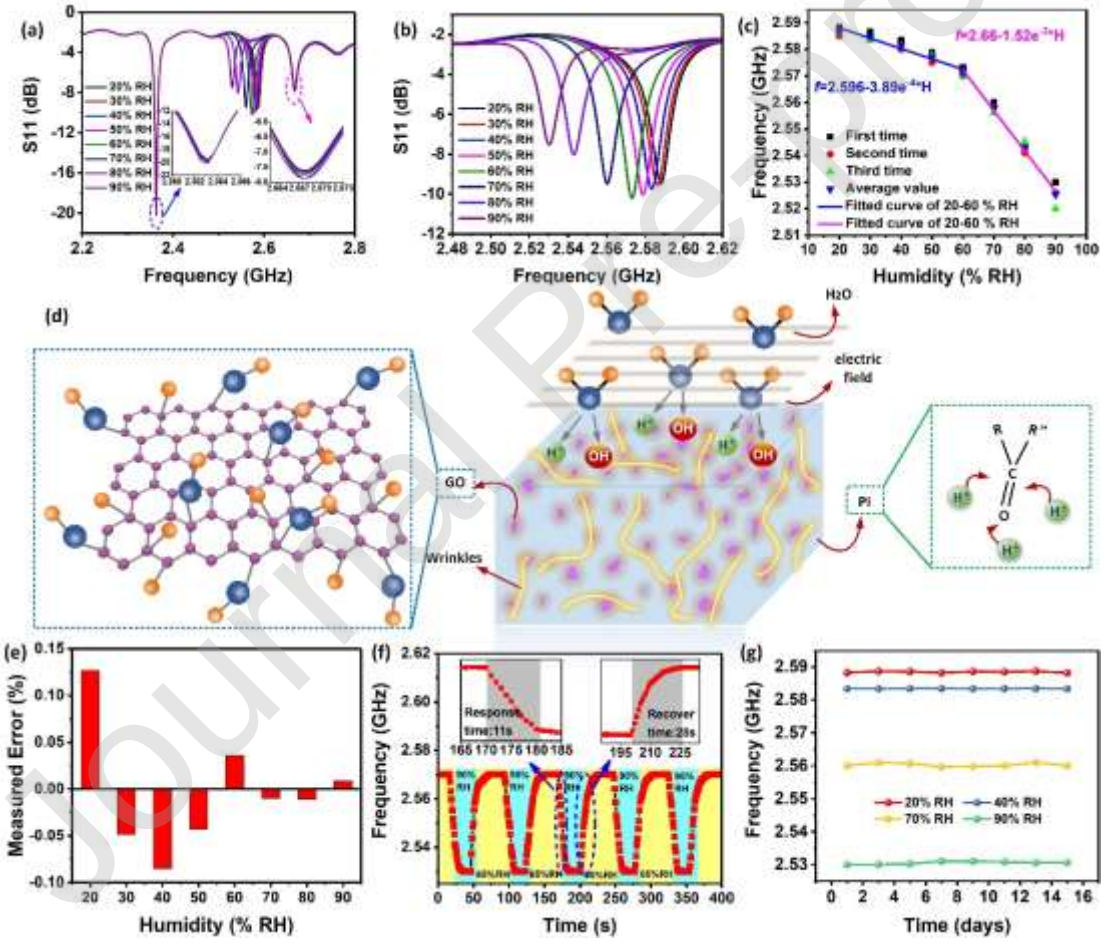

Figure 8.